



Lawrence Berkeley Laboratory

UNIVERSITY OF CALIFORNIA

ENERGY & ENVIRONMENT DIVISION

Presented at the General Motors Research Laboratory Conference,
Particulate Carbon: Atmospheric Life Cycle, Warren, MI
October 12-14, 1980

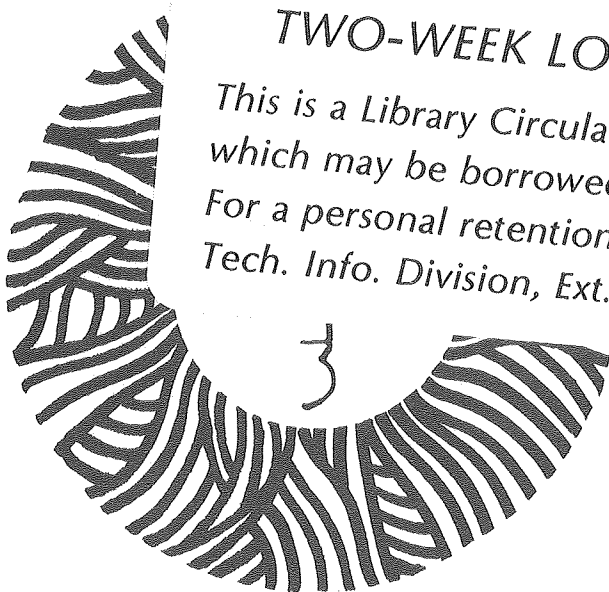
CHEMICAL AND CATALYTIC PROPERTIES OF ELEMENTAL CARBON

S.G. Chang, R. Brodzinsky, L.A. Gundel, and T. Novakov

October 1980

TWO-WEEK LOAN COPY

*This is a Library Circulating Copy
which may be borrowed for two weeks.
For a personal retention copy, call
Tech. Info. Division, Ext. 6782.*



RECEIVED
LIBRARY
OCT 15 1980

LIBRARY AND
DOCUMENTS SECTION

LBL-11678 c.2

DISCLAIMER

This document was prepared as an account of work sponsored by the United States Government. While this document is believed to contain correct information, neither the United States Government nor any agency thereof, nor the Regents of the University of California, nor any of their employees, makes any warranty, express or implied, or assumes any legal responsibility for the accuracy, completeness, or usefulness of any information, apparatus, product, or process disclosed, or represents that its use would not infringe privately owned rights. Reference herein to any specific commercial product, process, or service by its trade name, trademark, manufacturer, or otherwise, does not necessarily constitute or imply its endorsement, recommendation, or favoring by the United States Government or any agency thereof, or the Regents of the University of California. The views and opinions of authors expressed herein do not necessarily state or reflect those of the United States Government or any agency thereof or the Regents of the University of California.

CHEMICAL AND CATALYTIC PROPERTIES OF ELEMENTAL CARBON*

S.G. Chang, R. Brodzinsky, L.A. Gundel, and T. Novakov
Lawrence Berkeley Laboratory
University of California
Berkeley, California 94720

Introduction

Elemental carbon particles resulting from incomplete combustion of fossil fuel are one of the major constituents of airborne particulate matter [1,2]. These particles are a chemically and catalytically active material and can be an effective carrier for other toxic air pollutants through their adsorptive capability. The chemical, adsorptive, and catalytic behaviors of carbon particles depend very much on their crystalline structure, surface composition, and electronic properties. This paper discusses these properties and examines their relevance to atmospheric chemistry.

Structure

The diameter of elemental carbon particles varies from 50 Å or even smaller to several thousand Å. The results of X-ray diffraction [3] have shown that each particle is made up of a large number of crystallites 20 to 30 Å in diameter. Each crystallite consists of several carbon layers with a graphitic hexagonal structure, having defects, dislocations, and discontinuities in the layer planes, and thus containing high concentrations of unpaired electrons which constitute the active sites. Carbon atoms located at these sites show strong tendencies to react with other molecules because of residual valencies. During particle formation, interactions of air, water, flue gas, etc., with carbon particles occur, resulting in the incorporation of oxygen, hydrogen, and

*This work was supported by the Biomedical and Environmental Research Division of the U.S. Department of Energy under contract no. W-7405-ENG-48 and by the National Science Foundation.

nitrogen into the structure. Therefore, elemental carbon particles may be regarded as a complex three-dimensional organic polymer with the capability of transferring electrons, rather than merely as an amorphous form of elemental carbon.

Surface Complexes

Surface complexes may determine the adsorptive, electrical, and catalytic properties of carbon particles [4]. It is therefore important to determine the structure of surface species. Many studies have been carried out in the past on the determination of surface oxygen species [5]. Nearly every type of oxygen-containing functional group known in organic chemistry has been postulated to exist on the carbon surface (Fig. 1). The functional groups most often suggested are carboxyl groups, phenolic hydroxyl groups, and quinone carbonyl groups [6-10]. Less often suggested are ether, peroxide, and ester groups in the forms of normal and fluorescein-like lactones [11], carboxylic acid anhydrides [12], and cyclic peroxide [13]. The relative amounts of these complexes and their structure depends on the thermal history of carbon particles [14-17].

Little is known about the structure of surface nitrogen species, although the capability of fixation of nitrogen [18] in carbon particles and the promoting effect of the catalytic activity of nitrogenous carbon [19] have been observed. We have investigated the structure of surface nitrogen complexes produced as a result of the reaction between carbon particles and NH_3 at both an oxidizing [1] and a reducing atmosphere.

The first set of experiments involves the exposure of combustion-produced soot with NH_3 in air. The nature of surface nitrogen species thus formed was studied with the aid of ESCA. Soot particles for these experiments were generated by a pre-mixed propane-oxygen flame. The exposure of soot particles

to NH_3 was done under two different experimental conditions: in a static regime, with propane soot precollected on a silver membrane filter subsequently exposed to the reactant gas at ambient temperature; and in a flow system, by introducing the reactant gas downstream from the propane-oxygen flame, i.e., while the soot particles are still at high temperature.

ESCA spectra of the nitrogen (1s) region of soot samples prepared in these ways are shown in Figs. 2 and 3. It is evident from Fig. 2 that interaction of NH_3 with "cold" soot particles results in ammonium-like species. However, as seen from Fig. 3, NH_3 interacting with "hot" soot particles produces species with ESCA peaks of binding energies designated as N_x species. Ammonium in these samples is probably produced on soot particles after they have been collected on the filter and cooled down.

Using ESCA, Novakov et al. [20] have observed, in addition to commonly occurring nitrate and ammonium, two reduced nitrogen species with N (1s) binding energy corresponding to N_x surface species produced under laboratory conditions. Chemical equivalency of ambient and synthetic N_x species is demonstrated by their thermal behavior. The experimental procedure is to measure ESCA spectra at gradually increasing sample temperatures. The results of such measurements for one ambient particulate sample, collected in Pomona, California, during a moderate smog episode (24 October 1972) and for a sample prepared by NH_3 -hot soot interaction are shown in Figs. 4 and 5.

The spectrum of the ambient sample (Fig. 4) at 25°C shows the presence of NO_3^- , NH_4^+ , and N_x . At 80°C the entire nitrate peak is lost, accompanied with a similar loss in ammonium peak intensity. The shaded portion of the ammonium peak in the 25°C spectrum represents the ammonium fraction volatilized between 25 and 80°C. It appears therefore that the nitrate in this sample is mainly in the form of ammonium nitrate. At 150°C the only nitrogen species remaining

is N_x . The ammonium fraction still present at 80°C but absent at 150°C is associated with some ammonium compound more stable than NH_4NO_3 , possibly ammonium sulfate. At 250°C the appearance of another peak, labeled N'_x , is seen. This peak continues to increase at 350°C. The total peak areas of spectra recorded at 150, 250, and 350°C remain constant, indicating that the N_x component is transformed into N'_x by heating in vacuum.

N_x species produced by surface reactions of hot soot with NH_3 have the same kind of temperature dependence as the ambient samples. This is illustrated in Fig. 5. The spectrum taken at room temperature shows that most nitrogen species in this sample are of the N_x type. Heating the sample in vacuum to 150°C does not influence the line shape or intensity. At 250°C, however, the formation of N'_x is evident. Further transformation of N_x to N'_x occurred at 350°C.

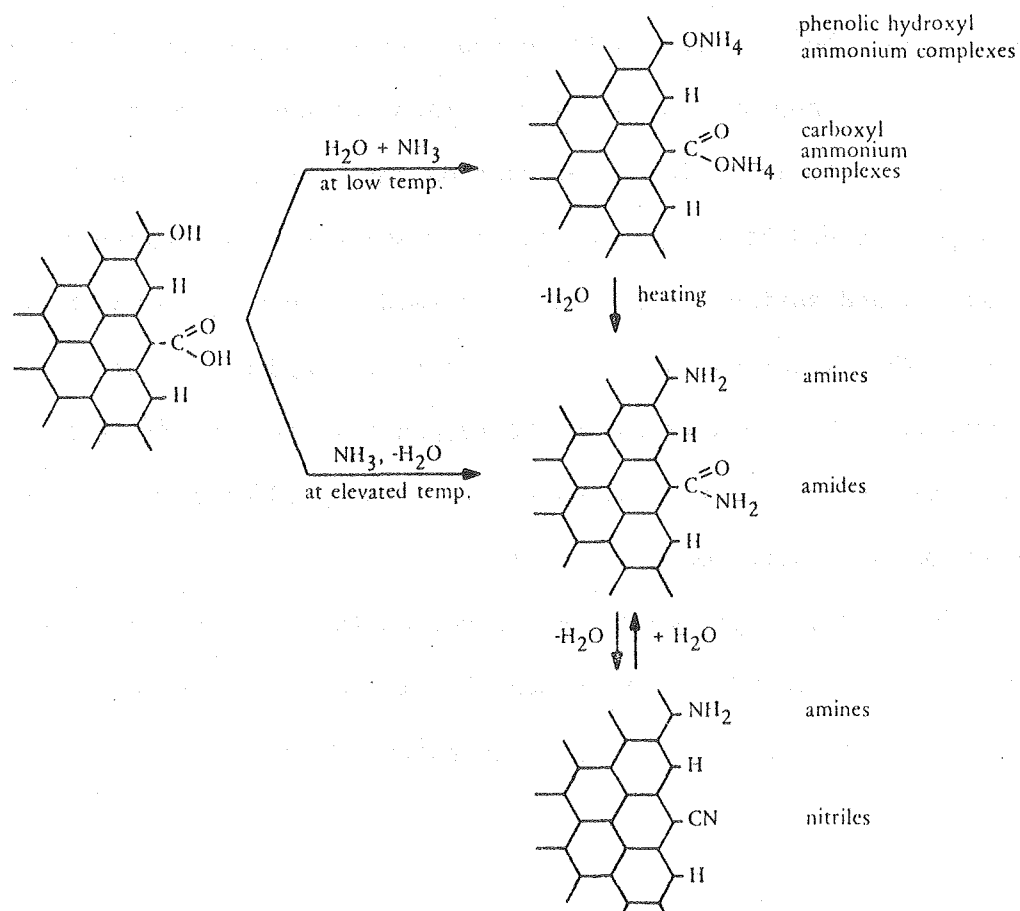
Both ambient and synthetic N'_x species will remain unaltered even if the temperature is lowered back to room temperature if the sample remains in vacuum. However, if the sample is taken out of vacuum and exposed to moisture, N'_x will be transformed back to the original N_x compound. It can be concluded that N'_x species are produced by dehydration of N_x .

The outlined results indicate that reduced nitrogen species of the N_x and N'_x type observed in ambient pollution particulates are chemically analogous to the reduced nitrogen species produced by surface reactions at elevated temperature of ammonia with finely divided carbon or soot. The same reactants at room temperature produce surface ammonium compounds.

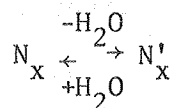
Based on these experimental results, N_x was assigned to a mixture of amines and amides, and N'_x to nitrile. Since prior to the interaction with NH_3 , the soot particle surface was in contact with air and flue gas, it therefore should be covered with surface oxygen complexes. By using the

most often-mentioned surface oxygen-carbon functional groups (i.e., carboxyl groups and phenolic hydroxyl groups) and in analogy with organic chemistry, we can describe some possible reactions of NH_3 and soot leading to the formation of amides, amines, nitriles, and ammonium-salt-like compounds associated with soot particle surfaces.

At low temperatures soot particles covered with surface carboxyl or phenolic groups may act as a Bronsted acid when interacting with NH_3 . Carboxyl ammonium or phenolic ammonium salts will be formed as the result of proton exchange. Ammonia may also be physically adsorbed by hydrogen bonding to surface OH or COOH groups. At elevated temperatures the carboxyl group carbon is electrophilic and has the tendency to accept an electron pair from the basic species in the process of coordination. The nucleophilic substitution reaction of NH_3 with carboxylic acid yields an amide which may dehydrate and become a nitrile upon further heating. Carboxyl and phenolic hydroxyl ammonium salts may dehydrate at elevated temperature to produce amides and/or nitriles and amines respectively.



The photoelectron spectroscopic results indicate that the amides and amines correspond to the N_x species. These appear as broad peaks indicating the presence of more than one chemical species. Nitriles formed from amides by dehydration on heating correspond to the N'_x species. We have established the reversibility of the



process. The carboxyl ammonium and phenolic hydroxyl ammonium salts produced by NH_3 chemisorption correspond to the volatile ambient ammonium species.

We have studied the stability of ambient particulate nitrogen in water by combining ESCA measurements with determination of total nitrogen by proton activation [21]. Our results with samples from several location (Berkeley, Los Angeles, and St. Louis) indicate that 1) a large fraction of N_x (85%) originally present in ambient particulate matter can be removed by water extraction; and 2) more NH_4^+ appears in the extract than was present on the untreated sample and less N_x appears in the extract than was present on the untreated sample. The N_x deficiency in the extract matches the surplus in NH_4^+ . The former behavior could be attributed to water-soluble stoichiometric compounds such as amines and surface species such as amides and nitrile which can undergo hydrolysis. The latter could be attributed to the hydrolysis of amide and nitrile groups. These behaviors may be responsible for the disagreement of chemical composition in black episodes with those predicted from the equilibrium phase diagram as constructed by Brosset [22].

The other set of experiments [23] involves the grinding of a purified grade POCO graphite in NH_3 in the absence of air at room temperature. The concentration of nitrogen with respect to carbon was determined by ESCA. The

information on the structure of surface nitrogen species was obtained with the aid of Fourier transform infrared spectroscopy. To help in the assignment of vibrational frequencies, infrared spectra of graphite particles after reaction with deuterated ammonia were also obtained.

The grinding reduced particle sizes and creates fresh surfaces. Surface carbon atoms of graphite particles show a strong chemical reactivity because of unsaturation in valency. Figures 6a and 6c show infrared spectra of the graphite particles after extensive grinding in an atmosphere of NH_3 and ND_3 , with expansions of these spectra in Figs. 6b and 6d. These infrared spectra suggest the occurrence of dissociative chemisorption of NH_3 on the carbon particle surface. Vibrational frequencies associated with the surface groups C-NH_2 , C=N-H , $\text{C}\equiv\text{N}$, and C-H are observed in Figs. 6a and 6b. The isotope shifts shown in Figs. 6c and 6d support these assignments. Surface CNH_2 groups give rise to two bands near 3400 cm^{-1} that are attributed to symmetric and anti-symmetric N-H stretching modes. These two bands should shift to 2500 cm^{-1} for CND_2 . This shift is shown in Figs. 6c and 6d. A NH_2 bending mode near 1580 cm^{-1} should shift to about 1200 cm^{-1} for the ND_2 groups. However, a strong band due to the $k=0, E_{2g}$ phonon mode of the graphite lattice [24] and/or a vibrational mode of the aromatic structure of graphite [25] also occurs at about 1580 cm^{-1} . Likewise, the C-N stretching mode vibrates at approximately 1200 cm^{-1} and appears in both the C-NH_2 and the C-ND_2 surface groups.

We have detected surface nitrogen groups indicating the dissociation of more than one bond in a molecule of ammonia. A band between 1600 and 1700 cm^{-1} could be assigned to immines (C=NH and C=N-C), a weak band at 2300 cm^{-1} to nitrile ($\text{C}\equiv\text{N}$), and one at 2180 cm^{-1} to isocyanide ($-\text{N}^+\equiv\text{C}^-$).

The evidence of the dissociative chemisorption of ammonia on carbon particle surfaces is also supported by the appearance of the C-D stretching band at 2050 cm^{-1} . The assignment of the C-H stretching is ambiguous because

the C-H stretching is near 2900 cm^{-1} where a vibrational band appears on both NH_3 and ND_3 samples. This band could be the overtone and/or combination bands resulting from the strong absorption band between 1300 and 1600 cm^{-1} . There is also a band, possibly of the same nature, at 2700 cm^{-1} in both samples.

Acidity

Depending on the thermal history or the condition of activation, elemental carbon particles may possess either acidic or basic character. Because of this property, soot may influence the pH of atmospheric water droplets [26]. It has been shown that activation of elemental carbon by exposure to O_2 at temperatures between 200 and 400°C produces an acidic type. By contrast, activation of carbon at high temperatures either in pure CO_2 or under vacuum, followed by exposure to oxygen at room temperature, results in a basic type.

The acidic character can be explained by the dissociation of acidic surface oxygen functional groups such as carboxyl and hydroxyl in solution. The nature of the basic character has been a topic of considerable discussion and controversy [27-32]. The idea of the presence of basic sites in the form of surface oxides has been proposed by Shilov and Chmutov [27] and Garten and Weiss [28], among others, to account for the chemisorption of acids. The latter suggested that the oxides were in the form of a chromene-like structure after neutralization with acid, which would result in the formation of carbonium ion. The presence of carbonium cationic sites on the surface of acid-treated carbon was confirmed by Rivin [29], but it could not be established whether the basic sites are due to the presence of the chromene-like surface oxides or the inherent property of the polynuclear aromatic structures of the carbon particles. Frumkin et al. [30] proposed an electrochemical theory in which the adsorption of the acids by carbon is determined by the electrical potential at the carbon solution interface and by the capacity of the double layer. According to

Steenberg [31], adsorption of acids involved primary adsorption of protons by physical force and secondary adsorption of anions in the diffuse double layer. On the contrary, Mattsen and Mark [32] attributed the neutralization of acids at high acid concentrations to the primary adsorption of the anions and secondary adsorption of the protons.

Catalysis

Elemental carbon particles are effective catalysts [33] for many different types of reactions including oxidation-reduction, halogenation, hydrogenation-dehydrogenation, dehydration, polymerization, and isomerization. Table I lists a few reactions catalyzed by carbon that could have direct bearing on atmospheric chemistry. It is difficult to assess the importance of all these reactions in the atmosphere at this time because useful rate equations have not been determined. We have recently performed a study [35, 36] on the kinetics and mechanism for the catalytic oxidation of SO_2 on carbon in aqueous suspensions and have obtained a rate equation applicable to atmospheric conditions. The reaction was studied by batch (flask) experiments, from which a rate law was derived. This rate law has been confirmed by fog chamber studies [46]. The flask experiments were performed using suspensions of commercially available activated carbons as well as suspensions of combustion-produced soots.

Figure 7 shows the typical reaction curves of the oxidation of S(IV) in aqueous suspensions of soot particles collected from acetylene and natural gas flames. The reaction occurs in two steps. The initial disappearance of S(IV) is so fast that its rate could not be followed by the analytical techniques used. The second step is characterized by a much slower reduction of S(IV). The results obtained with these combustion-produced soots were reproduced (Fig. 8) by suspensions of similar concentrations of one of the commercially available activated carbons (Nuchar C-190, a trademark of West Virginia Pulp and Paper

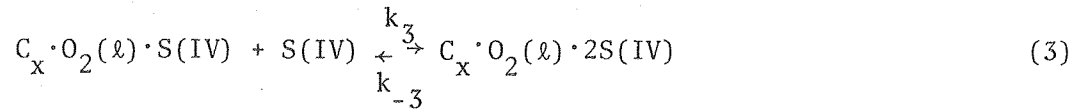
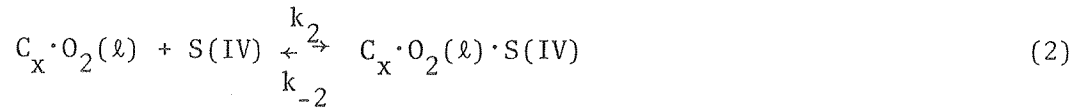
Co.). Figure 8 also shows a mass balance between the S(IV) consumed and the sulfate produced. At a constant temperature, the amount of S(IV) oxidized by the rapid first step process was found to be proportional to the carbon particle concentration.

The reaction of the second step has the following characteristics:

1. The reaction rate is independent of pH ($\text{pH} < 7.6$), and therefore $\text{SO}_2 \cdot \text{H}_2\text{O}$, HSO_3^- , and SO_3^{2-} are indistinguishable in terms of oxidation on the carbon surfaces.
2. The reaction is first order with respect to the concentration of carbon particles.
3. The activation energy of the reaction is ~ 8.5 kcal/mole, being slightly different for different carbons.
4. The reaction rate has a complex dependence on the concentration of S(IV), ranging between a second and zeroth order reaction as the S(IV) concentration increases.
5. The reaction rate has a complex dependence on the concentration of dissolved O_2 , with the order of reaction between zeroth and first.

Figure 9 shows the effective rate of reaction (normalized carbon concentration, room temperature - 20°C , and air) as a function of the sulfurous acid concentration for the activated carbons studied (see also Table II). From the Nuchar C-190 curve, the rate of reaction is second order with respect to S(IV) below 10^{-7} M, moves through a first order reaction around 5×10^{-6} M, and becomes independent of S(IV) concentrations above 10^{-4} M. The other curves are seen to be similar in their behavior.

Based on the experimental results, we propose the following reaction mechanism



where C_x = soot, $O_2(l)$ = dissolved oxygen molecule, $S(IV)$ = sulfite species, and $S(VI)$ = sulfate species.

Equation (1) indicates that dissolved oxygen is adsorbed on the soot particle surface to form an activated complex. This adsorbed oxygen complex then oxidizes the $S(IV)$ to form sulfate according to Equations (2)-(4). If one assumes that the reaction follows the condition of Langmuir adsorption equilibrium [47], the rate of acid formation is

$$\frac{d[S(VI)]}{dt} = 2k_4[C_x] \left(\frac{K_1[O_2]}{1 + K_1[O_2]} \right) \left(\frac{K_2[S(IV)]}{1 + K_2[S(IV)]} \right) \left(\frac{K_3[S(IV)]}{1 + K_3[S(IV)]} \right) \quad (I)$$

where $K_1 = k_1/k_{-1}$, $K_2 = k_2/k_{-2}$, $K_3 = k_3/k_{-3}$.

The experimental results yield the following rate law for this reaction:

$$\frac{d[S(VI)]}{dt} = k[C_x] \left(\frac{K[O_2]}{1 + K[O_2]} \right) f[S(IV)] \quad (IIa)$$

$$\text{where } f[S(IV)] = \left(\frac{\alpha[S(IV)]^2}{1 + \beta[S(IV)] + \alpha[S(IV)]^2} \right),$$

$[C_x]$ = grams of carbon particles per liter,

$[O_2]$ = moles of dissolved oxygen per liter, and

$[S(IV)]$ = total moles of S(IV) per liter.

For Nuchar C-190 the following constants were determined: $k = 0.874 e^{-4428/T}$ moles/g·sec ($T = ^\circ K$); $K_1 = 2.103 \times 10^3$ L/mole, $\alpha = 2.404 \times 10^{12}$ L²/mole², and $\beta = 1.219 \times 10^7$ L/mole.

We have previously reported [36] the experimental rate law for Nuchar C-190 in the form

$$\frac{d[S(VI)]}{dt} = k[C_x][O_2]^{0.69} f[S(IV)] \quad , \quad (IIb)$$

where $k = 9.04 \times 10^3 e^{-5888/T}$ moles^{.31}·L^{.69}/g·sec, and the numerical values for α and β were slightly different. The current values for the activation energy, α , and β were calculated after submission of our previous work with more recent data.

Equation (IIb) can be changed simply to Equation (IIa). A fractional order adsorption reaction is achieved by substituting the Freundlich isotherm $\theta = k[X]^n$, where θ is the fraction of the surface covered by adsorbed species X, for the Langmuir [47] $\theta = K[X]/(1 + K[X])$. Multiplication of the S(IV) terms in Eq. (I) yields the experimentally seen expression, where $K_2 K_3 = \alpha$ and $K_2 + K_3 = \beta$.

The dependence of the rate of formation of sulfate on the partial pressure of SO₂ (P_{SO_2}) in the atmosphere can be obtained from Eq. (II). Because the effect of P_{SO_2} on the rate is contained in $f[S(IV)]$, we illustrate the relationship of $f[S(IV)]$ with P_{SO_2} and pH of the aqueous droplets as shown in Figs. 10 and 11. $f[S(IV)]$, or the rate of production of sulfate (because the rate is linearly proportional to $f[S(IV)]$), decreases as the pH decreases at a

given P_{SO_2} . The magnitude of $f[S(IV)]$'s changing per unit pH change is much larger at a lower P_{SO_2} . Also $f[S(IV)]$ (or the rate) depends only slightly on P_{SO_2} under most atmospheric conditions when P_{SO_2} is between 1 and 10 ppb and the pH ranges between 5 and 6. $f[S(IV)]$ increases only 1/10 and twofold respectively at pH of 6 and 5 when P_{SO_2} increases from 1 to 10 ppb. However, $f[S(IV)]$ depends strongly on P_{SO_2} when the pH is low.

The catalytic oxidation of sulfurous acid on carbon particles of different origins shows the same kinetic behavior. However, the rate constants of several different types of carbon particles were studied and found to differ from type to type. In principle, the reaction rate should be proportional to the concentration of active sites on the carbon particles, rather than to the concentration of carbon particles. The number of active sites per unit mass of carbon particles is different from type to type and is not necessarily proportional to the surface area. Sidelewski [48] has shown, by means of the electron paramagnetic resonance method, that free electrons on carbon particles can serve as active centers for the adsorption of oxygen molecules and for the oxidation of SO_2 . The concentration of free electrons is related to the origin and thermal history of the carbon particles.

It is therefore impractical to formulate a generally applicable rate constant for atmospheric soot particles because these particles may arise from the combustion of different types of fossil fuel under different combustion conditions and thus possess a different catalytic activity.

We have carried out a box-type calculation [35,37] to compare the relative importance of sulfate production mechanisms by soot particles with other mechanisms involving liquid water. The systems considered in the batch reactor include the SO_2 - CO_2 - $H_2O(l)$ -air and any of the oxidizing agents such as O_2 , O_3 , HNO_2 , or catalysts such as Fe^{+++} , Mn^{++} , and soot. The role of NH_3 is

investigated in these reactions. The kinetic results of Chang et al. [37,49], Beilke et al. [50], Erickson et al. [51], Freiberg [52], and Matteson et al. [53] for nitrous acid, oxygen, ozone, iron, and manganese systems respectively were used in this calculation.

All the oxidation mechanisms considered except Mn^{++} are pH dependent. Most of these mechanisms have lower oxidation rates at a lower pH, but some are more sensitive to the change in pH than others. The HNO_2 mechanism shows a larger oxidation rate when the solution is more acidic, however. The following initial conditions were used in the calculation: liquid water, 0.05 g/m^3 ; SO_2 , 0.01 ppm; O_3 , 0.05 ppm; and CO_2 , 0.000311 atm. Concentrations of particulate Fe and Mn of 250 ng/m^3 and 20 ng/m^3 respectively were assumed. However, only 0.13% of the total iron and 0.25% of the manganese are water soluble, according to Gordon et al. [54]. The concentration of soot and HNO_2 were taken as $10 \text{ } \mu\text{g/m}^3$ and 8 ppb respectively. The latter corresponds to 25 ppb of NO and 50 ppb of NO_2 at equilibrium conditions. For NH_3 a concentration of 5 ppb was used, which is higher than the highest equilibrium partial pressure of NH_3 over the United States as calculated by Lau and Charlson [55]. Tables III and IV list the equilibrium equations and oxidation rate equations used for this comparative study.

The following assumptions were made in the calculations:

1. The size of liquid water drops suspended inside the box is so small that the absorption rate of gaseous species (SO_2 , NH_3 , and HNO_2) is governed by chemical reactions.
2. There is no mass transfer of any species across the box during the reaction; therefore, the SO_2 (and NH_3 or HNO_2) in each box is depleted with time. The mass balance of the SO_2 , CO_2 , NH_3 , and HNO_2 is always maintained (i.e., $\Delta[\text{SO}_2]_{\text{g}} = \Delta[\text{SO}_2 \cdot \text{H}_2\text{O}] + \Delta[\text{HSO}_3^-] + \Delta[\text{SO}_3^{2-}] + \Delta[\text{HSO}_4^-] + \Delta[\text{SO}_4^{2-}]$; $\Delta[\text{CO}_2]_{\text{g}} =$

$\Delta[\text{CO}_2 \cdot \text{H}_2\text{O}] + \Delta[\text{HCO}_3^-] + \Delta[\text{CO}_3^{-2}]; \Delta[\text{NH}_3]_{\text{g}} = \Delta[\text{NH}_3 \cdot \text{H}_2\text{O}] + \Delta[\text{NH}_4^+];$ and $\Delta[\text{HNO}_2]_{\text{g}} = \Delta[\text{HNO}_2] + \Delta[\text{NO}_2^-] + 2\Delta[\text{N}_2\text{O}]_{\text{g}};$ all units are in mole).

3. The growth of liquid water droplets due to the vapor pressure lowering effect of the sulfuric acid formed in the droplets is neglected.

The rate of sulfate production is determined by a calculation scheme involving a combination of equilibrium and kinetic steps. Equilibrium between SO_2 in the gas phase and sulfur (IV) in the droplet is several orders of magnitude faster than oxidation of sulfur (IV) to sulfate [56]. Similar assumptions were made regarding NH_3 and CO_2 gases. Therefore, initially gases are taken to be in equilibrium with the aerosols. Then the formation of sulfate proceeds by the given time-dependent production rate. The increase in the sulfate level in the small time step Δt causes the reduction in pH of the solution, which in turn disturbs the equilibrium between the aerosol and its surrounding gaseous environment. More gases are dissolved in the aerosol to maintain the equilibrium. At the same time, these gases are depleted in the surrounding atmosphere. After each calculation, the time step is adjusted and the process is repeated until a 24-hour period is completed. The results are shown in Fig. 12.

Figure 12 indicates that O_3 , soot, and HNO_2 can be important mechanisms for sulfate aerosol formation. In general the O_3 mechanism is more important under high pH and/or photoactivity conditions when the concentration of O_3 is high, whereas both soot and HNO_2 processes are more important when the lifetime of fog or clouds is long and the pH of the droplets is low. Both soot and HNO_2 processes can be dominant processes close to sources and in heavily polluted urban areas, where the concentrations of soot and NO/NO_2 are high and the pH of aqueous droplets is low.

The rate constant for atmospheric soot particles varies, depending on the nature and history of particle production as discussed previously. In a fog

chamber study, Benner et al. [46] have recently found that the reaction rate of soot particles from a natural gas diffusion flame can be considerably faster than the reaction rate reported here. More determination of rate constants of soot from different types of fuel is therefore warranted.

References

1. S.G. Chang and T. Novakov, Atmos. Environ. 9, 495 (1975).
2. H. Rosen, A.D.A. Hansen, L. Gundel, and T. Novakov, Appl. Opt. 17, 3859 (1978).
3. U. Hofmann and D. Wilm, Z. Elektrochem. angew. physik. Chem. 42, 504 (1936).
4. V.A. Garten and D.E. Weiss, Rev. Pure Appl. Chem. 7, 69 (1957).
5. H.P. Boehm, Advan. Catalysis 16, 179 (1966).
6. R.W. Coughlin and F.S. Ezra, Environ. Sci. Technol. 2, 291 (1968).
7. B.R. Puri, in Chemistry and Physics of Carbon, Vol. VI (New York, Dekker, 1970), p. 191.
8. B.R. Puri, Carbon 4, 391 (1966).
9. R.N. Smith, Quarterly Rev. 13, 287 (1959).
10. Y.A. Zary'yanz, V.F. Kiselev, N.N. Lezhnev, and D.V. Nikitina, Carbon 5, 127 (1967).
11. V.A. Garten, D.E. Weiss, and J.B. Willis, Aust. J. Chem. 10, 295 (1957).
12. H.P. Boehm, E. Diehl, W. Heck, and R. Sappok, Angew. Chem. Int. Ed. Engl. 3, 669 (1964).
13. B.R. Puri, in, Proceedings, Conference on Carbon, 5th, Vol. 1 (Oxford, Pergamon, 1962), p. 165.
14. P.J. Hart, F.J. Vastola, and P.L. Walker, Jr., Carbon 5, 363 (1967).
15. N.R. Laine, F.J. Vastola, and P.L. Walker, Jr., J. Phys. Chem. 67, 2030 (1963).
16. H.B. Palmer and C.F. Cullis, in Chemistry and Physics of Carbon, Vol. 1 (New York, Dekker, 19), p. 265.
17. S.W. Weller and T.F. Young, J. Am. Chem. Soc. 70, 4155 (1948).
18. P.H. Emmett, Chem. Rev. 43, 69 (1948).
19. E.C. Larsen and J.H. Walton, J. Phys. Chem. 44, 70 (1940).

20. T. Novakov, P. Mueller, A.E. Alcocer, and J.W. Otvos, *J. Colloid Interface Sci.* 39, 225 (1972).
21. L.A. Gundel, S.G. Chang, M.S. Clemenson, S.S. Markowitz, and T. Novakov, in Nitrogenous Air Pollutants (Ann Arbor, Ann Arbor Science, 1979), p. 211.
22. C. Brosset, paper presented at the Chemical Institute of Canada Annual Meeting, Ottawa, Ontario, June 8-11, 1980, sessions on acid precipitation.
23. T. Novakov and S.G. Chang, Lawrence Berkeley Laboratory Report LBL-6323 (1977).
24. F. Tuinstra and J.L. Koenig, *J. Chem. Phys.* 53, 1126 (1970).
25. R.A. Friedel and L.J.E. Hofer, *J. Phys. Chem.* 74, 2921 (1970).
26. S.G. Chang and T. Novakov, Lawrence Berkeley Laboratory Report LBL-4446 (1975).
27. N. Shilov and K. Chmutov, *Z. Phys. Chem. (Leipzig)* A149, 211 (1930).
28. V.A. Garten and D.E. Weiss, *Aust. J. Appl. Sci.* 7, 148 (1956).
29. D. Rivin, in Proceedings of the 5th Conference on Carbon, Vol. II (New York, Pergamon, 1963), p. 199.
30. A. Frumkin, R. Burstein, and P. Lewin, *Z. Phys. Chem.* A157, 442 (1931).
31. B. Steenberg, Adsorption and Exchange of Ions on Activated Charcoal (Uppsala, Almquist and Wiksells, 1944).
32. J.S. Mattson and H.B. Mark, Jr., Activated Carbon, Ch. 6 (New York, Marcel Dekker, 1971).
33. R.W. Coughlin, *I&EC Product Research and Development* 8, 12 (1969).
34. T. Novakov, S.G. Chang, and A.B. Harker, *Science* 186, 259 (1974).
35. S.G. Chang, R. Brodzinsky, R. Toossi, S.S. Markowitz, and T. Novakov, in Proceedings, Conference on Carbonaceous Particles in the Atmosphere, Lawrence Berkeley Laboratory Report LBL-9037 (1979), p. 122.
36. R. Brodzinsky, S.G. Chang, S.S. Markowitz, and T. Novakov, Lawrence Berkeley Laboratory Report LBL-10488; accepted for publication in *J. Phys. Chem.* (1980).

37. S.G. Chang, R. Toossi, and T. Novakov, Lawrence Berkeley Laboratory Report LBL-11380; accepted for publication in Atmos. Environ. (1980).
38. W.R. Coffey III, D.R. Schryer, and R.S. Rogowski, Atmos. Environ. 14, 571 (1980).
39. L.G. Britton and A.G. Clarke, Atmos. Environ. 14, 829 (1980).
40. W.R. Cofer III, D.R. Schryer, and R.S. Rogowski, submitted for publication in Atmos. Environ. (1980).
41. M.N. Rao and O.H. Hougen, Chem. Eng. Progr. Symp. Series 48, 110 (1952).
42. P.F. Bente and J.H. Walton, J. Phys. Chem. 47, 133 (1943).
43. R. Dulou, Chim. Ind. (Paris) 54, 396 (1945).
44. E.Z. Stumpp, Anorg. allgem. Chem. 337, 292 (1965).
45. L. Gundel, private communication (1979).
46. W.H. Benner, private communication (1980).
47. A. Clark, The Theory of Adsorption and Catalysis (New York, Academic, 1970).
48. J. Siedlewski, Int. Chem. Eng. 5, 297 (1965).
49. S.B. Oblath, S.S. Markowitz, T. Novakov, and S.G. Chang, Lawrence Berkeley Laboratory Report LBL-10504; accepted for publication in J. Phys. Chem. (1980).
50. S. Beilke, D. Lamb, and J. Müller, Atmos. Environ. 9, 1083 (1975).
51. R.E. Erickson, L.M. Yates, R.L. Clark, and D. McEwen, Atmos. Environ. 11, 813 (1977).
52. J. Freiberg, Atmos. Environ. 9, 661 (1975).
53. M.J. Matteson, W. Stöber, and H. Luther, Ind. & Eng. Chem. Fundam. 8, 677 (1969).
54. G.E. Gordon, D.D. Davis, G.W. Israel, H.E. Landsberg, and T.C. O'Haver, Report NSF/RA/E-73/189 (1975); available from NTIS as PB 262 574).
55. N.C. Lau and R.J. Charlson, Atmos. Environ. 11, 475 (1977).
56. S. Beilke and G. Gravenhorst, Atmos. Environ. 14, 463 (1978).

Table I. Some reactions catalyzed by carbon.

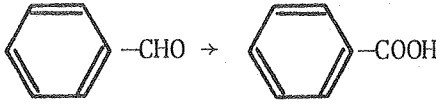
Reactions	References
1. $\text{SO}_2 + 1/2 \text{O}_2 \rightarrow \text{SO}_3$	Novakov et al. [34], Chang et al. [35], Brodzinsky et al. [36], Chang et al. [37]
2. $\text{SO}_2 + \text{NO}_2 \rightarrow \text{SO}_3 + \text{NO}$	Cofer et al. [38], Britton and Clarke [39]
3. $\text{SO}_2 + \text{O}_3 \rightarrow \text{SO}_3 + \text{O}_2$	Cofer et al. [40]
4. $\text{NO} + 1/2 \text{O}_2 \rightarrow \text{NO}_2$	Rao and Hougen [41]
5. $2\text{H}_2\text{O}_2 \rightarrow 2\text{H}_2\text{O} + \text{O}_2$	Bente and Walton [42]
6. $\text{CO} + \text{Cl}_2 \rightarrow \text{COCl}_2$	Dulou [43]
7. $\text{SO}_2 + \text{Cl}_2 \rightarrow \text{SO}_2\text{Cl}_2$	Dulou [43]
8. $\text{HCOOH} \begin{cases} \rightarrow \text{H}_2\text{O} + \text{CO} \\ \rightarrow \text{H}_2 + \text{CO}_2 \end{cases}$	Stumpp [44]
9. 	Gundel [45]
10. Hydroquinone \rightarrow quinhydrone \rightarrow quinone	Bente and Walton [42]

Table II. Summary of kinetic data for the catalytic oxidation of SO_2 by various elemental carbon particles in aqueous suspension.

Reaction rate equation:

$$\frac{d[\text{SO}_4^{-2}]}{dt} = A e^{-E_a/RT} [C_x] \left\{ \frac{K_1 [\text{O}_2]}{1 + K_1 [\text{O}_2]} \right\} \left\{ \frac{\alpha [\text{S(IV)}]^2}{1 + \beta [\text{S(IV)}] + \alpha [\text{S(IV)}]^2} \right\}$$

Kinetic data \ Elemental carbon	Nuchar C-190 (WESVACO)	Nuchar SN (WESVACO)	Aktivkohle (MERCK)
A (moles/g-sec)	0.874	0.158	2.473
E_a (kcal/mole)	8.8	8.1	8.8
K_1 (l/mole)	2.103×10^3	7.427×10^3	4.372×10^3
α (l ² /mole ²)	2.404×10^{12}	4.915×10^8	9.519×10^{11}
β (l/mole)	1.219×10^7	2.956×10^5	3.738×10^7

Table III. Chemical equilibrium constants at 25°C.^a

$\text{H}_2\text{O} \xrightleftharpoons{K_w} \text{H}^+ + \text{OH}^-$	$K_2 = 1.0008 \times 10^{-14}$
$\text{CO}_2(\text{g}) + \text{H}_2\text{O}(\text{l}) \xrightleftharpoons{H_c} \text{CO}_2 \cdot \text{H}_2\text{O}$	$H_c = 3.4 \times 10^{-2}$
$\text{CO}_2 \cdot \text{H}_2\text{O} \xrightleftharpoons{K_{1c}} \text{HCO}_3^- + \text{H}^+$	$K_{1c} = 4.45 \times 10^{-7}$
$\text{HCO}_3^- \xrightleftharpoons{K_{2c}} \text{CO}_3^{2-} + \text{H}^+$	$K_{2c} = 4.68 \times 10^{-11}$
$\text{NH}_3(\text{g}) + \text{H}_2\text{O}(\text{l}) \xrightleftharpoons{H_a} \text{NH}_3 \cdot \text{H}_2\text{O}$	$H_a = 57$
$\text{NH}_3 \cdot \text{H}_2\text{O} \xrightleftharpoons{K_a} \text{NH}_4^+ + \text{OH}^-$	$K_a = 1.774 \times 10^{-5}$
$\text{SO}_2(\text{g}) + \text{H}_2\text{O}(\text{l}) \xrightleftharpoons{H_s} \text{SO}_2 \cdot \text{H}_2\text{O}$	$H_s = 1.24$
$\text{SO}_2 \cdot \text{H}_2\text{O} \xrightleftharpoons{K_{1s}} \text{HSO}_3^- + \text{H}^+$	$K_{1s} = 1.7 \times 10^{-2}$
$\text{HSO}_3^- \xrightleftharpoons{K_{2s}} \text{SO}_3^{2-} + \text{H}^+$	$K_{2s} = 6.24 \times 10^{-8}$
$\text{HSO}_4^- \xrightleftharpoons{K_{3s}} \text{H}^+ + \text{SO}_4^{2-}$	$K_{3s} = 1.2 \times 10^{-2}$
$\text{HNO}_2(\text{g}) + \text{H}_2\text{O} \xrightleftharpoons{H_N} \text{HNO}_2 \cdot \text{H}_2\text{O}$	$H_N = 5.1 \times 10^{-4}$
$\text{HNO}_2 \cdot \text{H}_2\text{O} \xrightleftharpoons{K_N} \text{H}^+ + \text{NO}_2^-$	$K_N = 5.1 \times 10^{-4}$
$\text{O}_2 + \text{H}_2\text{O} \xrightleftharpoons{H_{O_2}} \text{O}_2 \cdot \text{H}_2\text{O}$	$H_{O_2} = 1.08 \times 10^{-3}$
$\text{O}_3 + \text{H}_2\text{O} \xrightleftharpoons{H_{O_3}} \text{O}_3 \cdot \text{H}_2\text{O}$	$H_{O_3} = 1.23 \times 10^{-2}$

^aConcentrations in moles/l and gas pressure in atm.

Table IV. Rate of SO₂ oxidation by various mechanisms in aqueous droplets.

Mechanism	Reaction rate law ^a
O ₂	Rate = $\frac{H_S \{k_2 + k_{10} K_W / [H^+]\} K_2 S k_3}{k_{-2} [H^+]^2 + k_{-10} [H^+] + K_2 S k_3} P_{SO_2}$
O ₃	Rate = $\{k_4 [HSO_3^-] + k_5 [SO_3^{2-}]\} [O_3 \cdot H_2O]$
Fe ⁺⁺⁺	Rate = $\frac{k_0 k_S^2 H_S^2 P_{SO_2}^2 [Fe^{+++}]}{[H^+]^3}$
Mn ⁺⁺	Rate = $3.67 \times 10^{-3} [X] - 1.17 \{ [HSO_4^-] + [SO_4^{2-}] \}^2 \{ [Mn^{++}] - [X] \} \times [H_2O(l)]^{-2}$ where $X = \frac{k_1 H_S P_{SO_2} [Mn^{++}]}{k_1 \{ H_S P_{SO_2} + [H_2O(l)] [Mn^{++}] \} + 0.17}$
Soot	Rate = $k_6 [C_x] [O_2]^{.69} \frac{\alpha [S^{+4}]^2}{1 + \beta [S^{+4}] + \alpha [S^{+4}]^2}$
HNO ₂	Rate = $k_7 [H^+]^2 [NO_2^-] + k_8 [H^+] [NO_2^-] [HSO_3^-] + k_9 [NO_2^-] [HSO_3^-]^2$

^a [H₂O(l)] in cc/m³, concentration in mole/l, gas pressure in atm, and time in sec, $k_0 = 151.69$ l/mole-sec, $k_S = 1.84 \times 10^{-2}$ mole/l, $k_1 = 8.12 \times 10^4$ l/mole-sec, $k_2 = 3.4 \times 10^6$ sec⁻¹, $k_{-2} = 2 \times 10^8$ l/mole-sec, $k_{10} = 2.9 \times 10^5$ l/mole-sec, $k_{-10} = 2.3 \times 10^{-7}$ sec⁻¹, $k_3 = 1.7 \times 10^{-3}$ sec⁻¹, $k_4 = 1.1 \times 10^5$ l/mole-sec, $k_5 = 7.4 \times 10^8$ l/mole-sec, $k_6 = 1.2 \times 10^{-4}$ mole^{.3} · l^{.7}/g · sec, $\alpha = 1.5 \times 10^{12}$ l²/mole², $\beta = 3.06 \times 10^6$ l/mole, $k_7 = 8 \times 10^5$ l²/mole²-sec, $k_8 = 3.8 \times 10^3$ l²/mole²-sec, $k_9 = 9 \times 10^{-4}$ l²/mole²-sec.

Figure Captions

Figure 1. Oxygen-containing functional groups on elemental carbon particle surfaces.

Figure 2. Nitrogen (1s) ESCA spectrum of cold soot particles exposed to NH_3 .

The setup used for exposure is also shown.

Figure 3. Nitrogen (1s) ESCA spectrum of hot soot particles exposed to NH_3 .

The experimental arrangement used for sample preparation is also shown.

Figure 4. Nitrogen (1s) ESCA spectrum of an ambient sample as measured at 25, 80, 150, 250, and 350°C.

Figure 5. Nitrogen (1s) spectrum of (hot) soot sample exposed to NH_3 , as measured at 25, 150, 250, and 350°C.

Figure 6. Infrared spectra of the graphite particles after extensive grinding in an atmosphere of NH_3 (a) and ND_3 (c). (b) and (d) are 2X expansions along the ordinate of (a) and (c) respectively.

Figure 7. S(IV) concentration as a function of time for acetylene and natural gas soot suspensions.

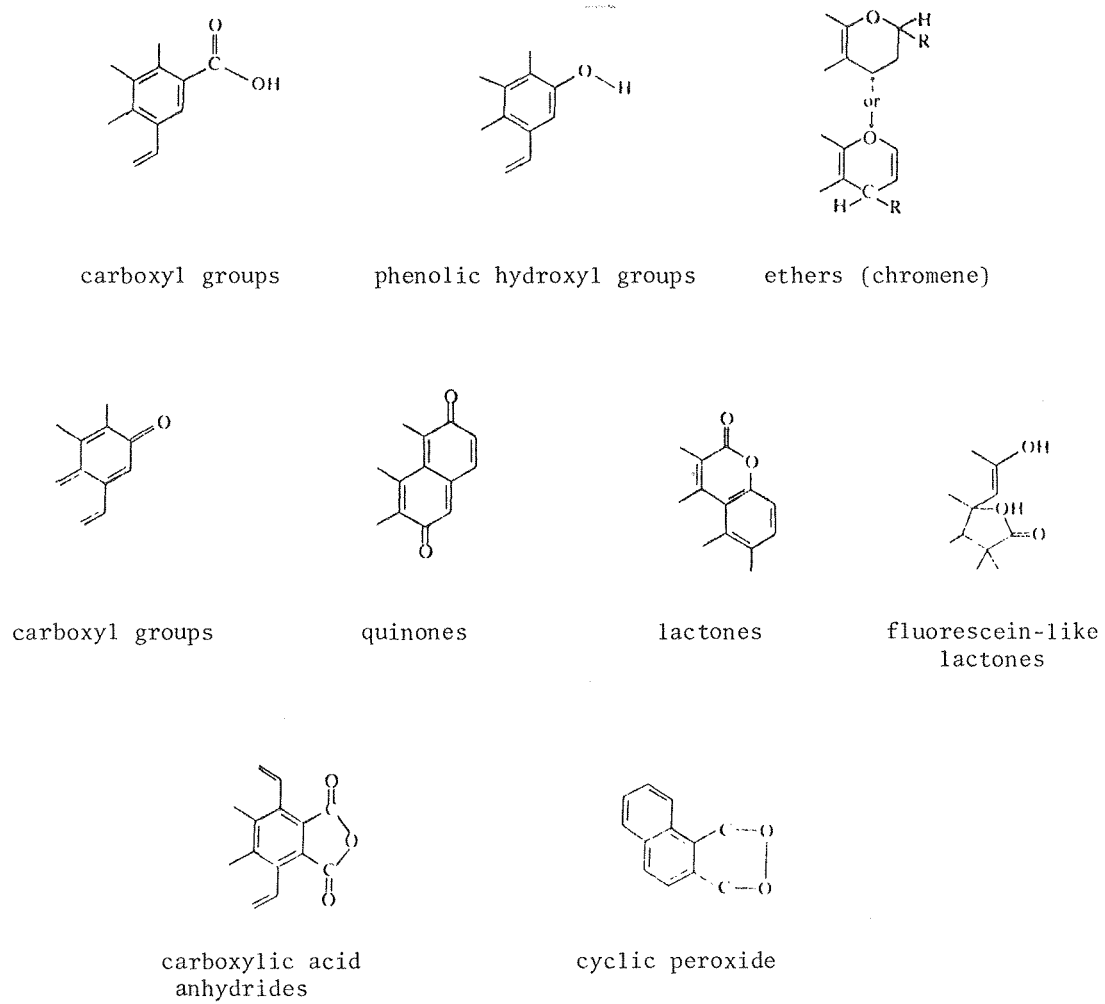
Figure 8. S(IV) and SO_4^{-2} concentrations as a function of time for a 0.16%-by-weight activated carbon suspension.

Figure 9. Effective rate of oxidation of S(IV) catalyzed on various activated carbon particles vs. S(IV) concentration.

Figure 10. The effect of the pH of aqueous droplets on $f[\text{S(IV)}]$ at $P_{\text{SO}_2} = 100$, 10, and 1 ppb. $f[\text{S(IV)}]$ is a function of S(IV) that the aqueous oxidation rate of sulfites on soot particles depends on.

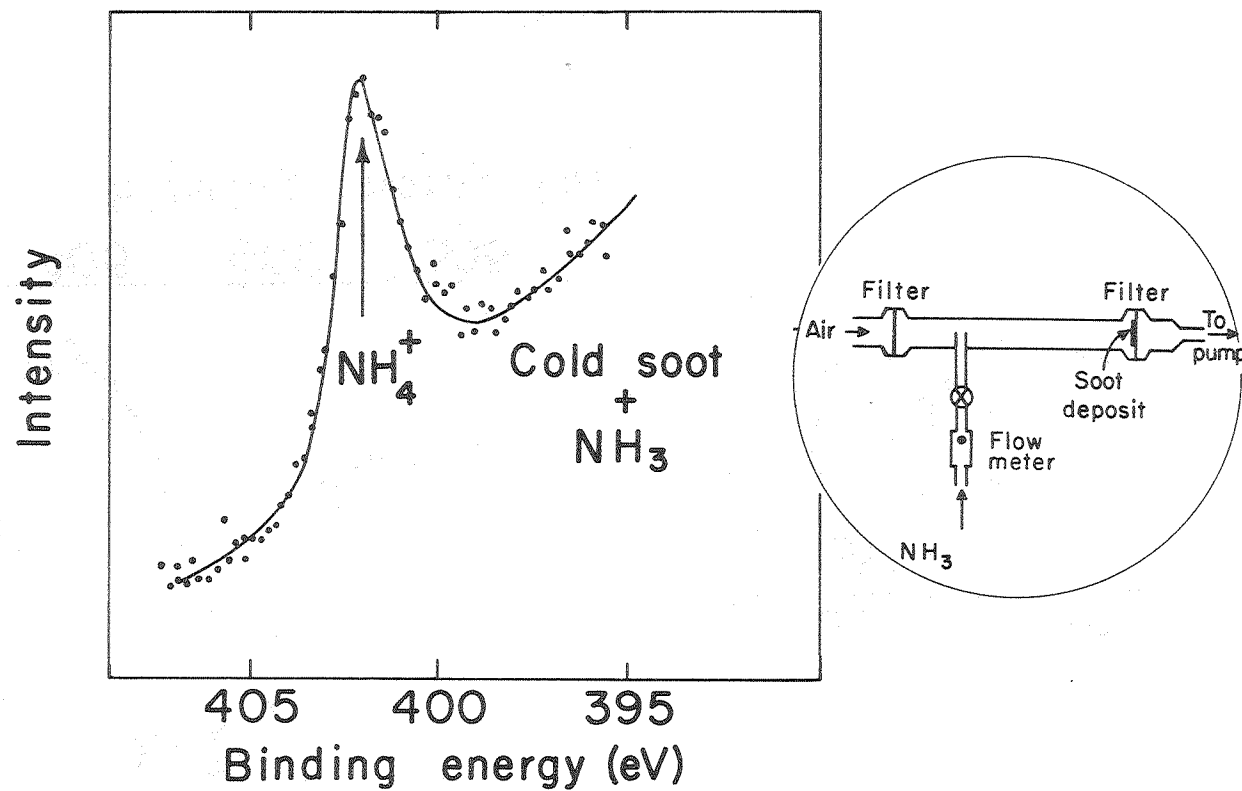
Figure 11. The effect of partial pressure of SO_2 on $f[\text{S(IV)}]$ at pH of 7, 6, 5, 4, and 3. $f[\text{S(IV)}]$ is a function of S(IV) that the aqueous oxidation rate of sulfites on soot particles depends on.

Figure 12. Comparison of the relative importance of various sulfate production mechanisms involving liquid water based on a box-type calculation. The following initial conditions were used in the calculation: $P_{SO_2} = 0.01$ ppm; $P_{CO_2} = 0.000311$ atm; $P_{NH_3} = 5$ ppb; $P_{O_3} = 0.05$ ppm; $P_{HNO_2} = 8$ ppb; $[Fe^{+3}] = 1.2 \times 10^{-7}$ mole/l; $[Mn^{+2}] = 1.8 \times 10^{-8}$ mole/l; soot = $10 \mu g/m^3$; and liquid water = $0.05 g/m^3$.



XBL 8010-12445

Figure 1



XBL 8010-12443

Figure 2

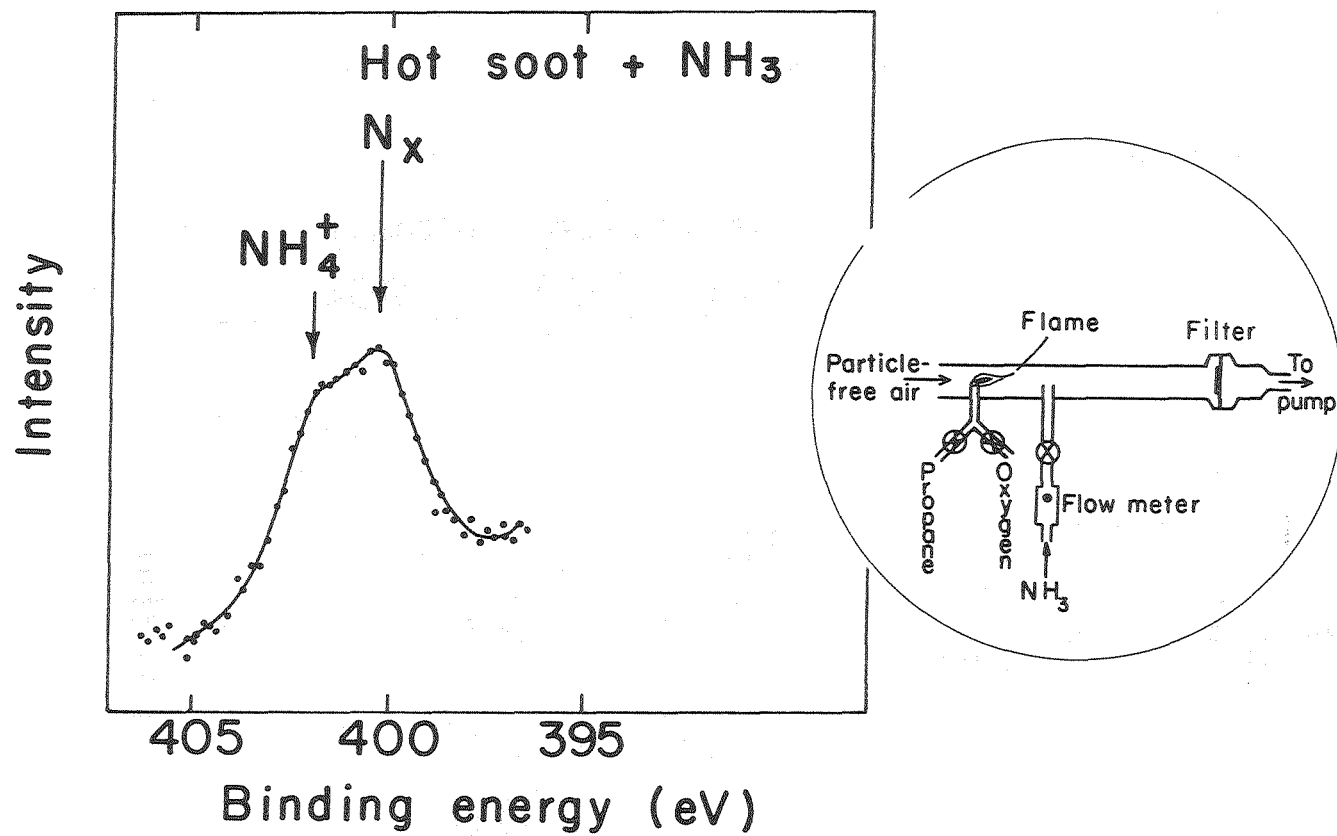
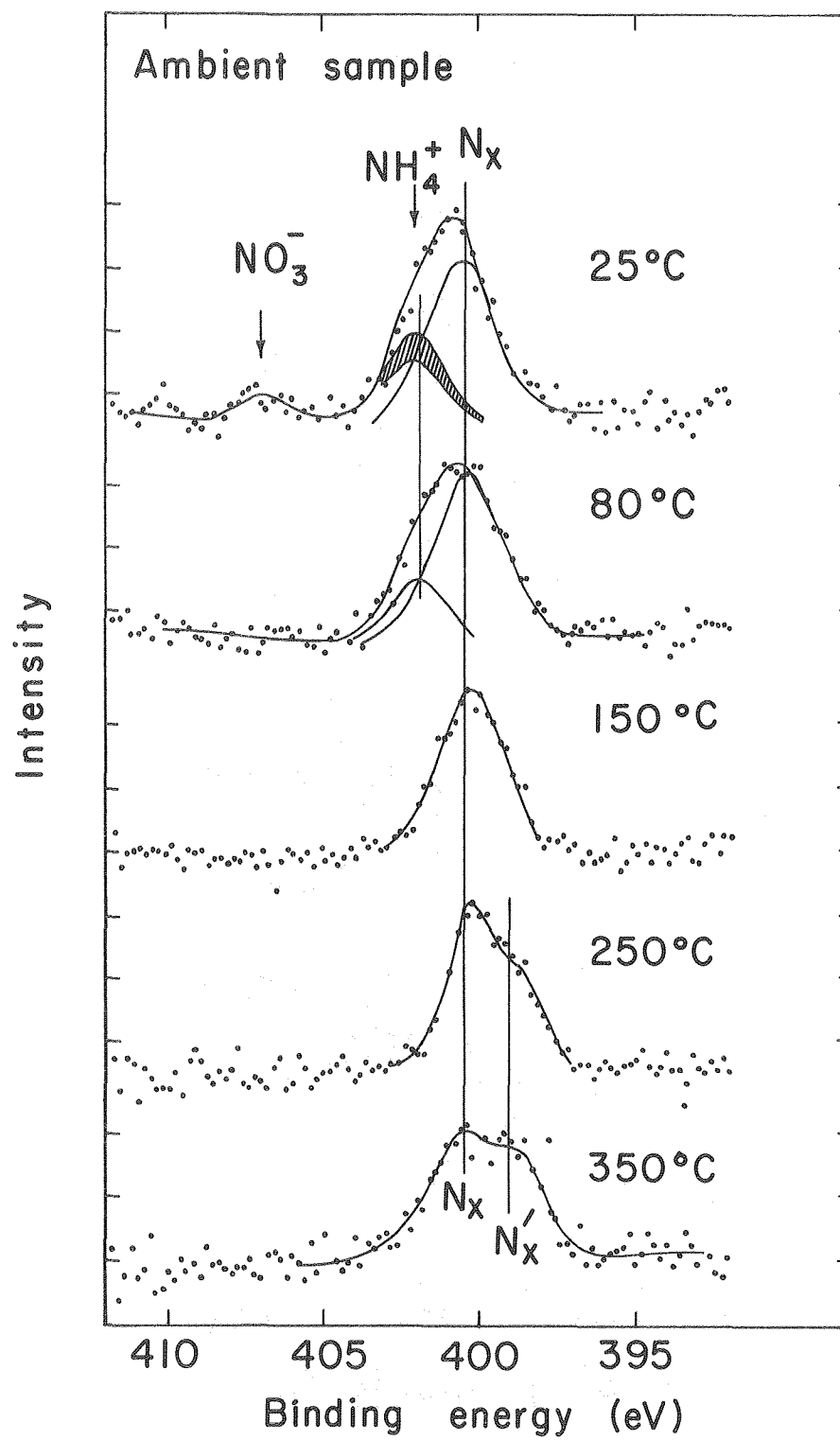


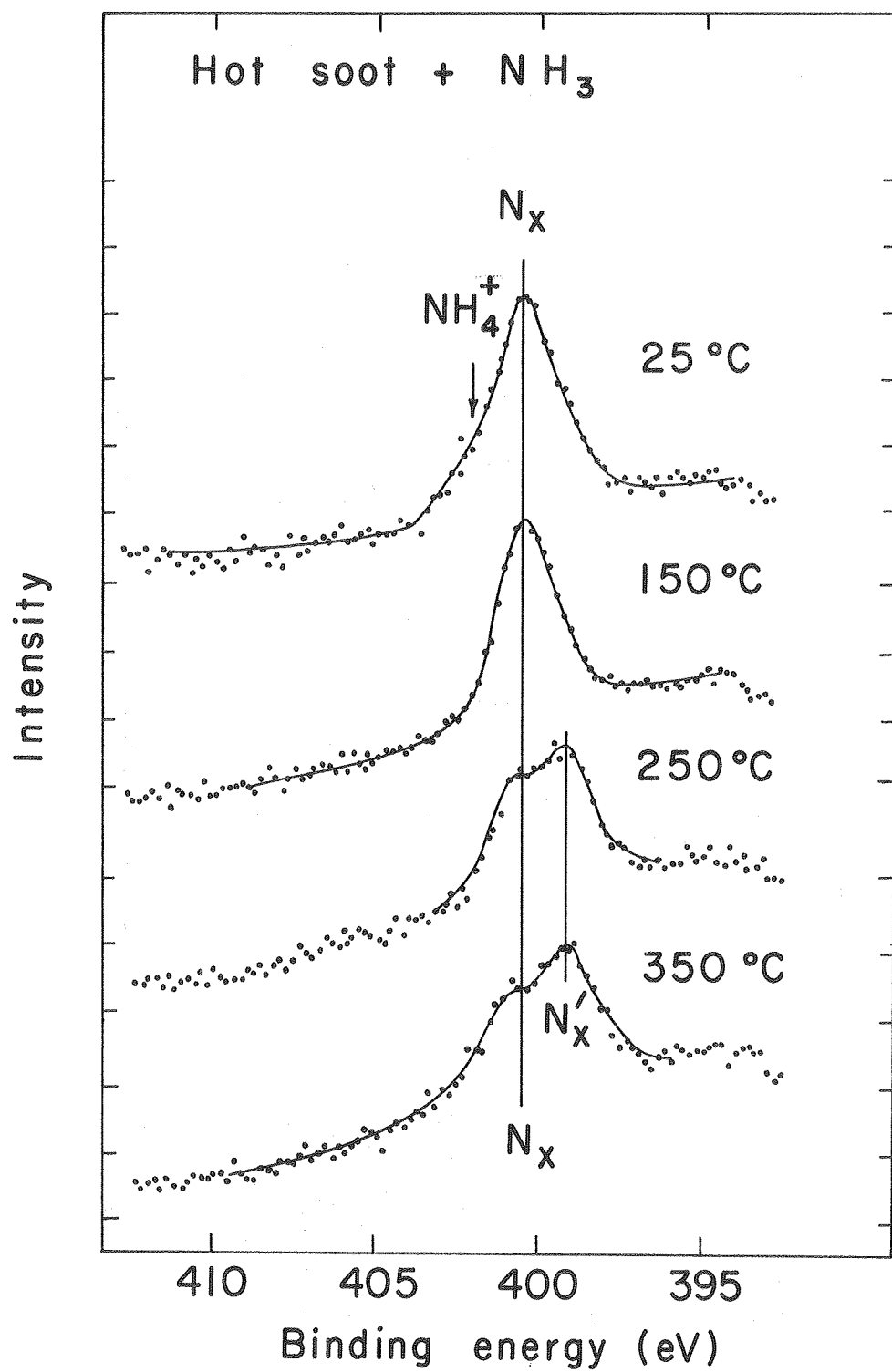
Figure 3

XBL 8010-12441



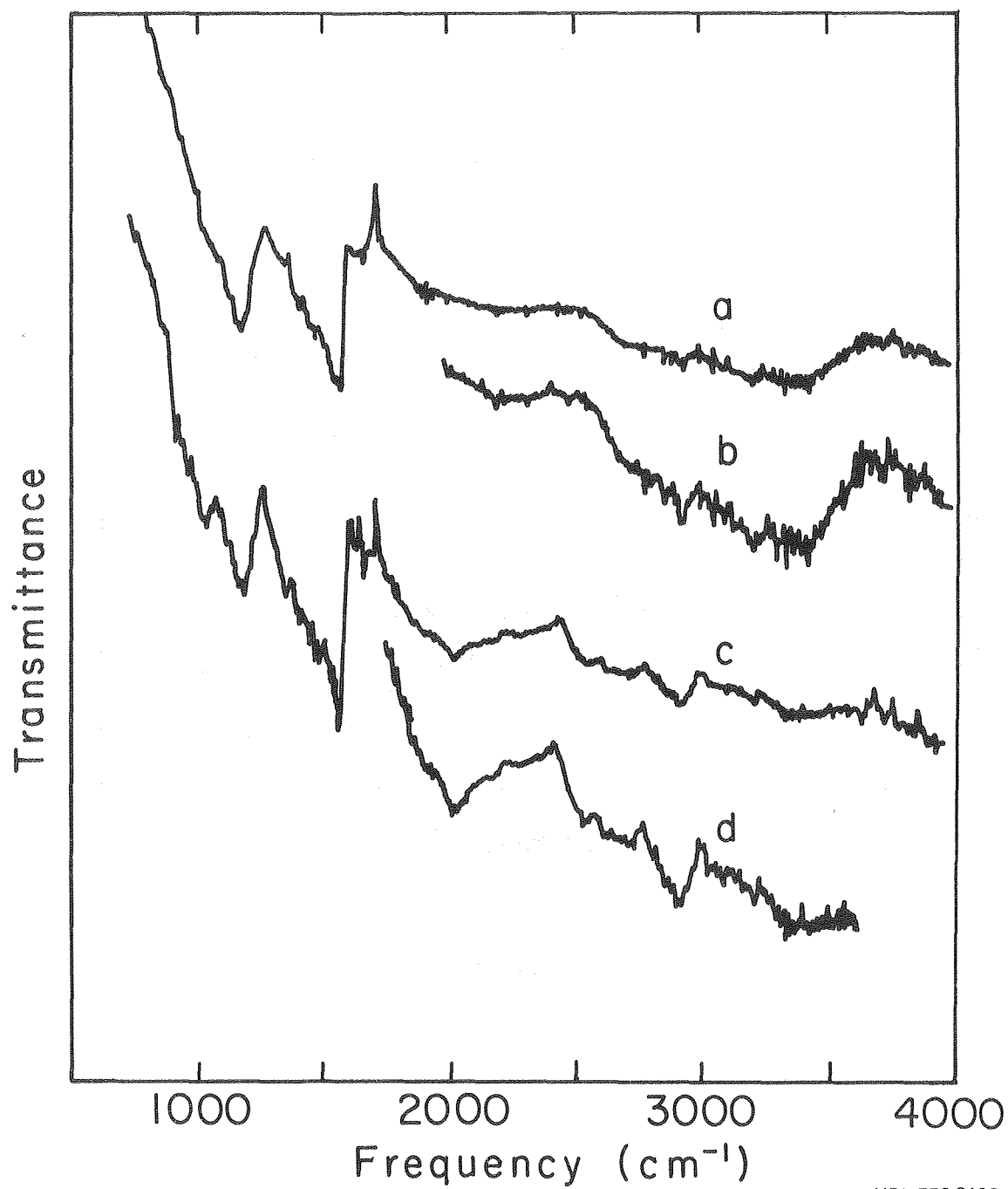
XBL746-3532

Figure 4



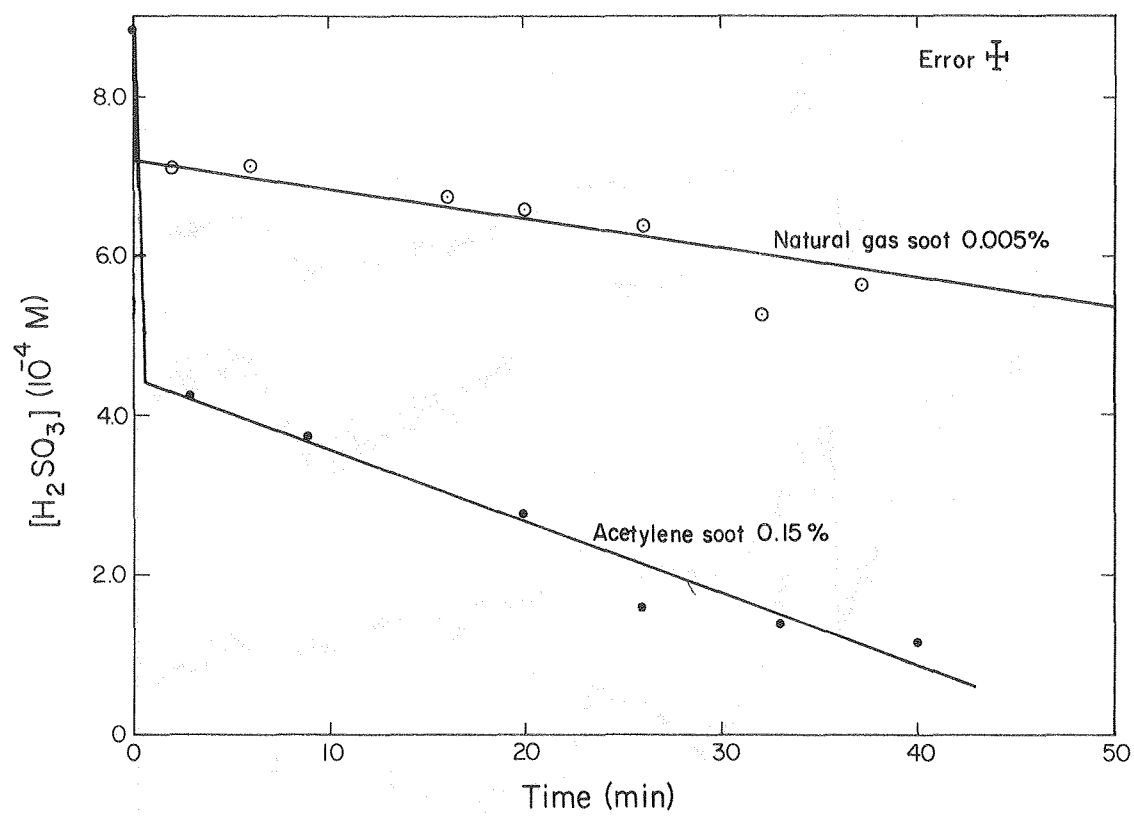
XBL746-3531

Figure 5



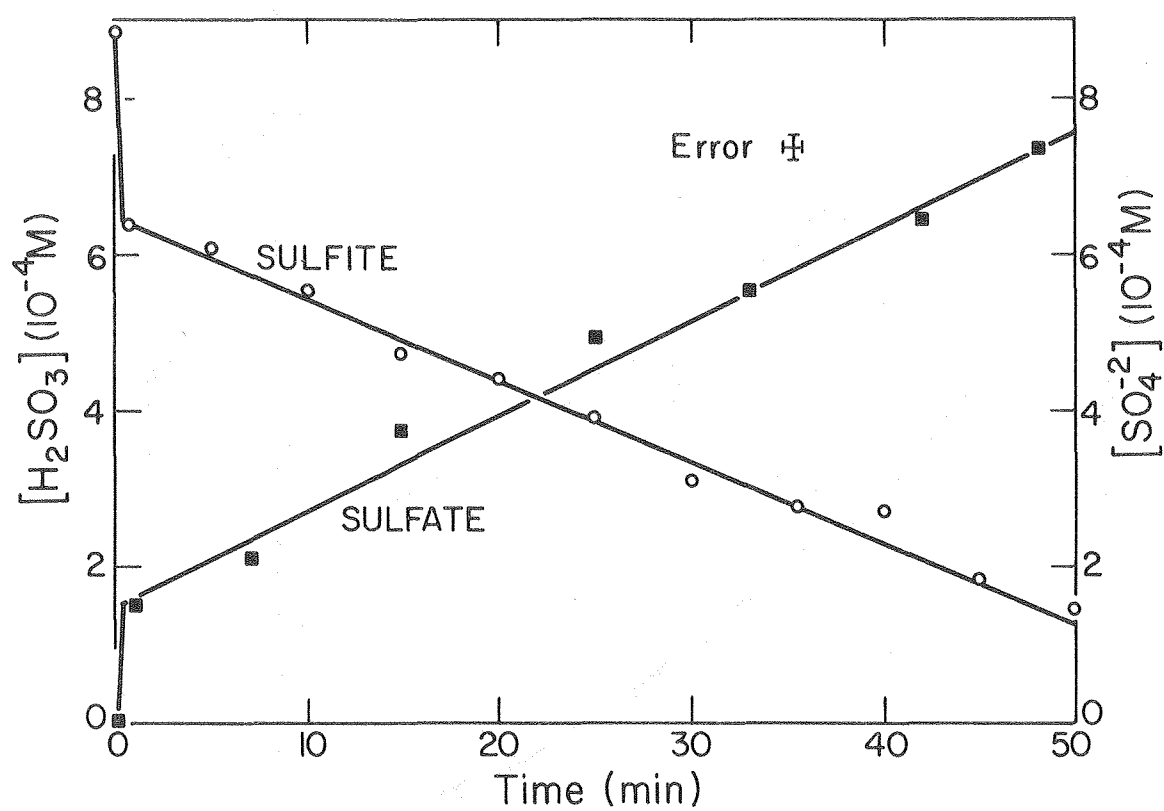
XBL 773-8123

Figure 6



XBL7710-2065A

Figure 7



XBL 782-219

Figure 8

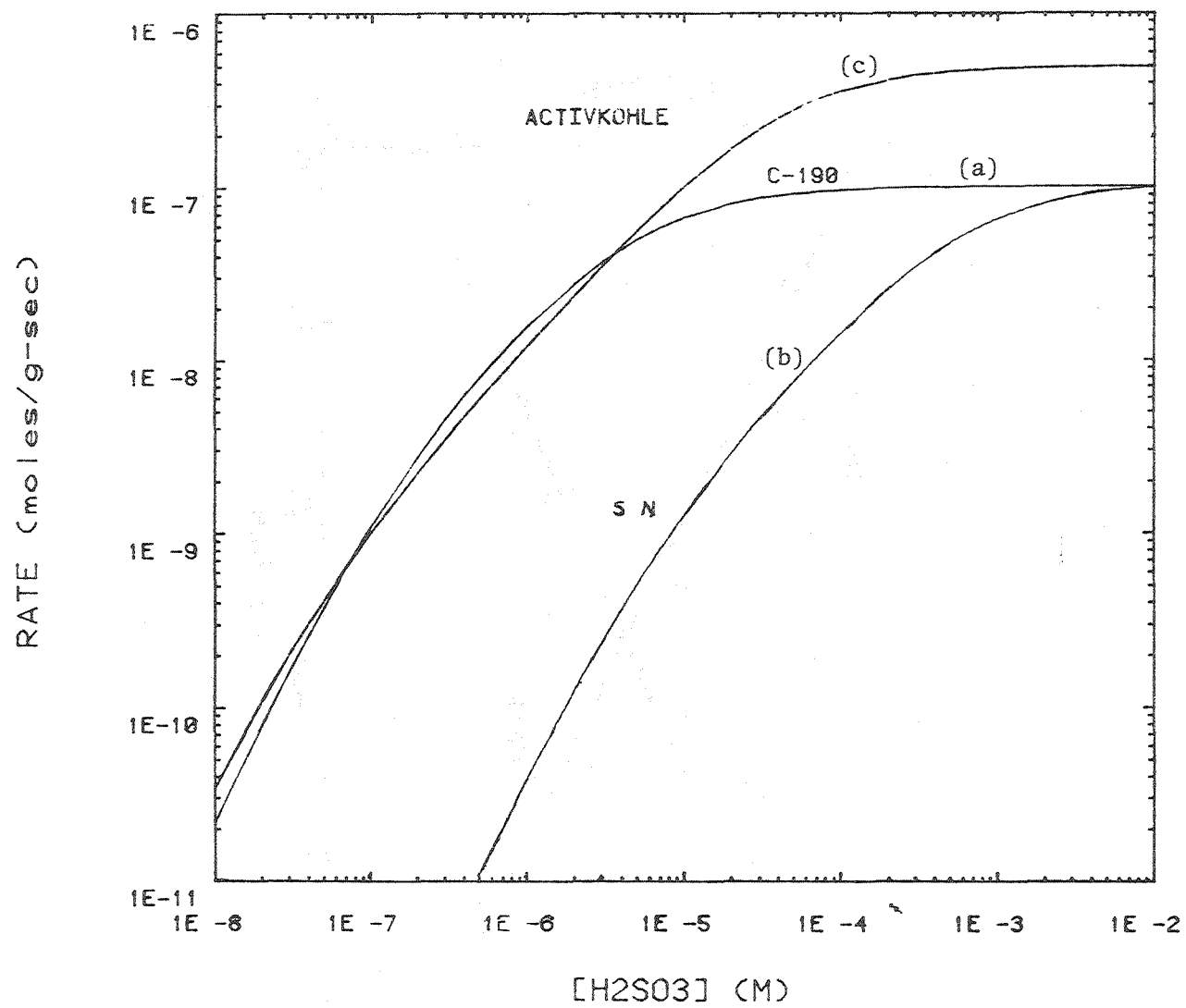
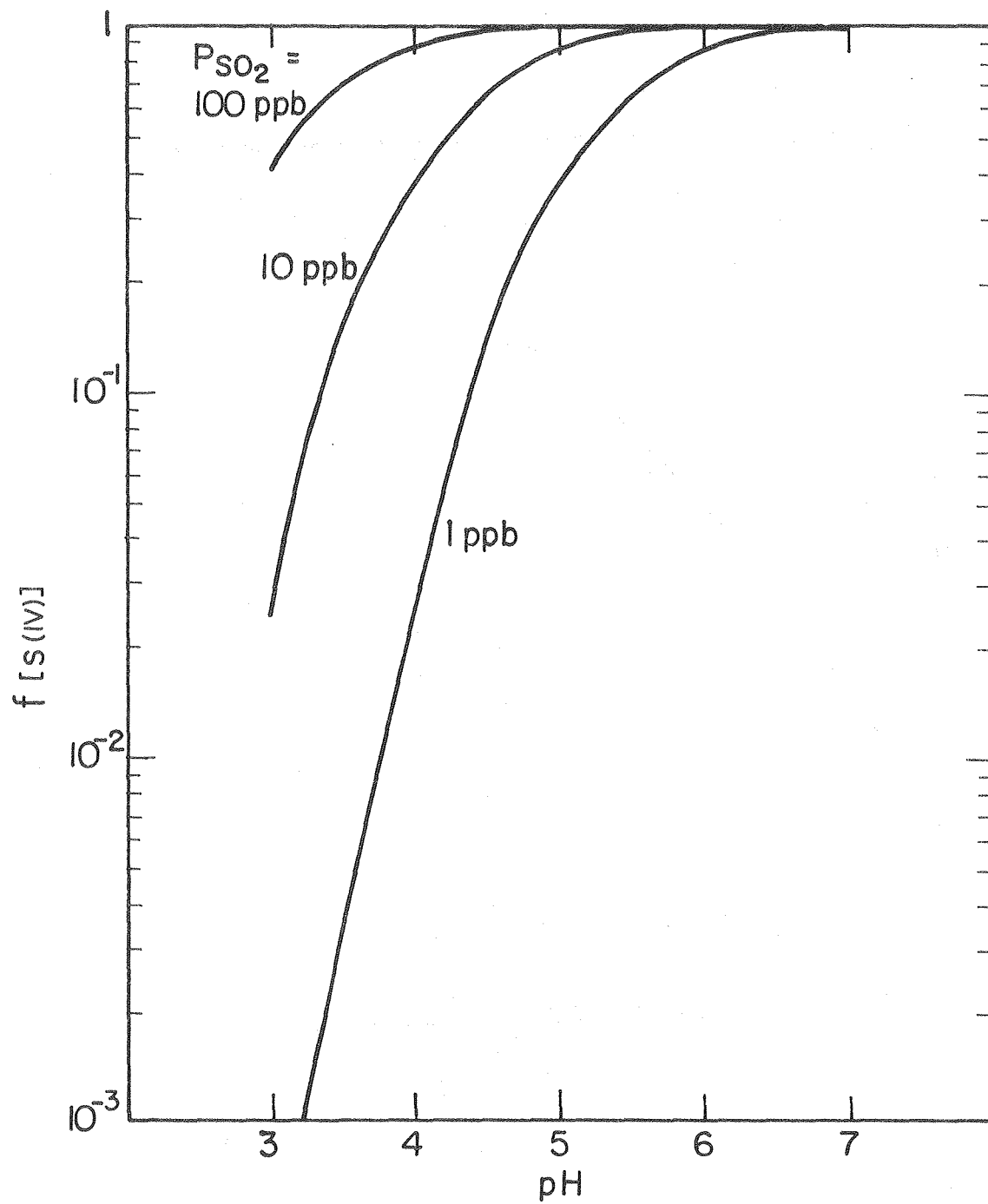


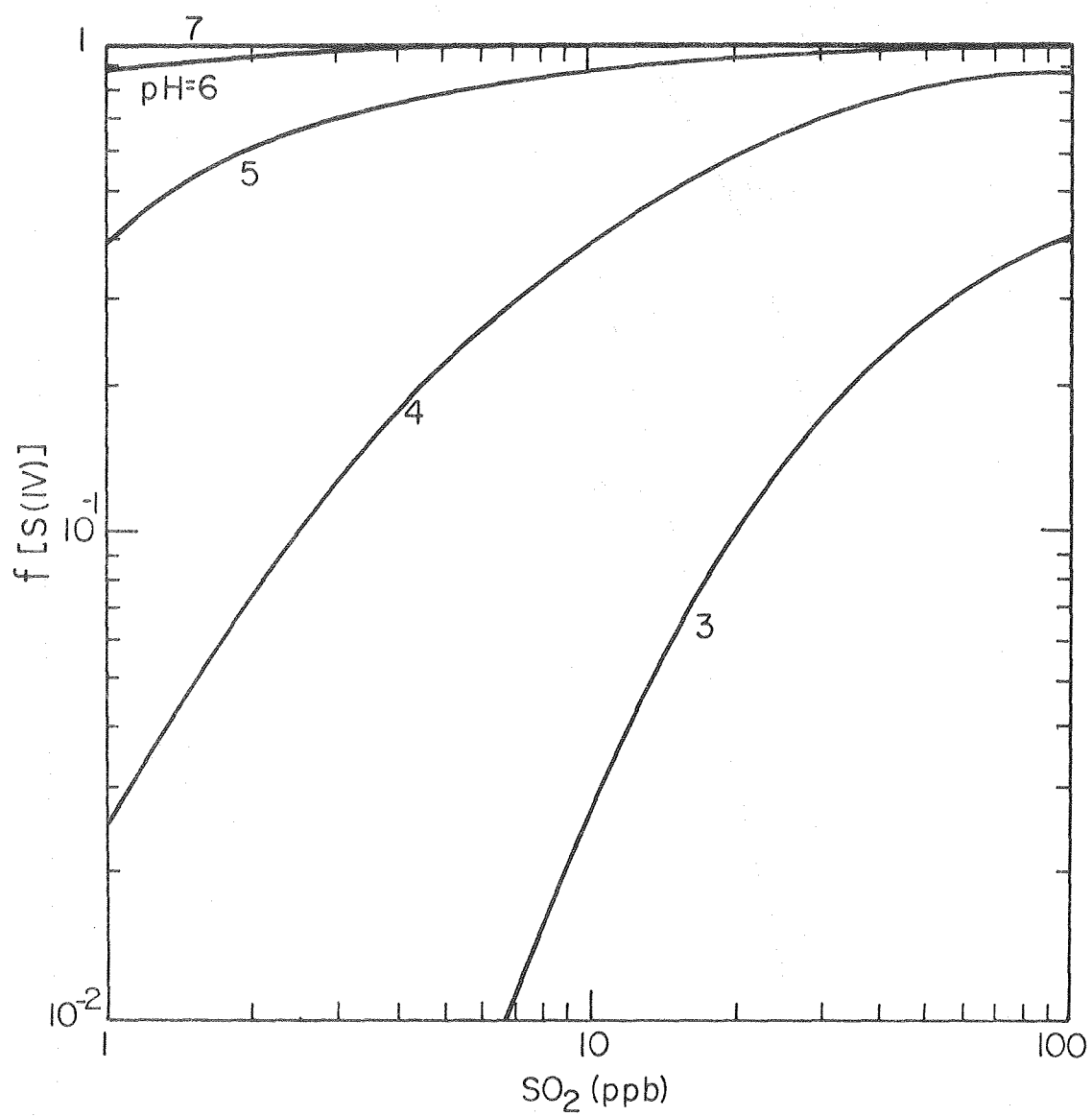
Figure 9

XBL 8010-12442



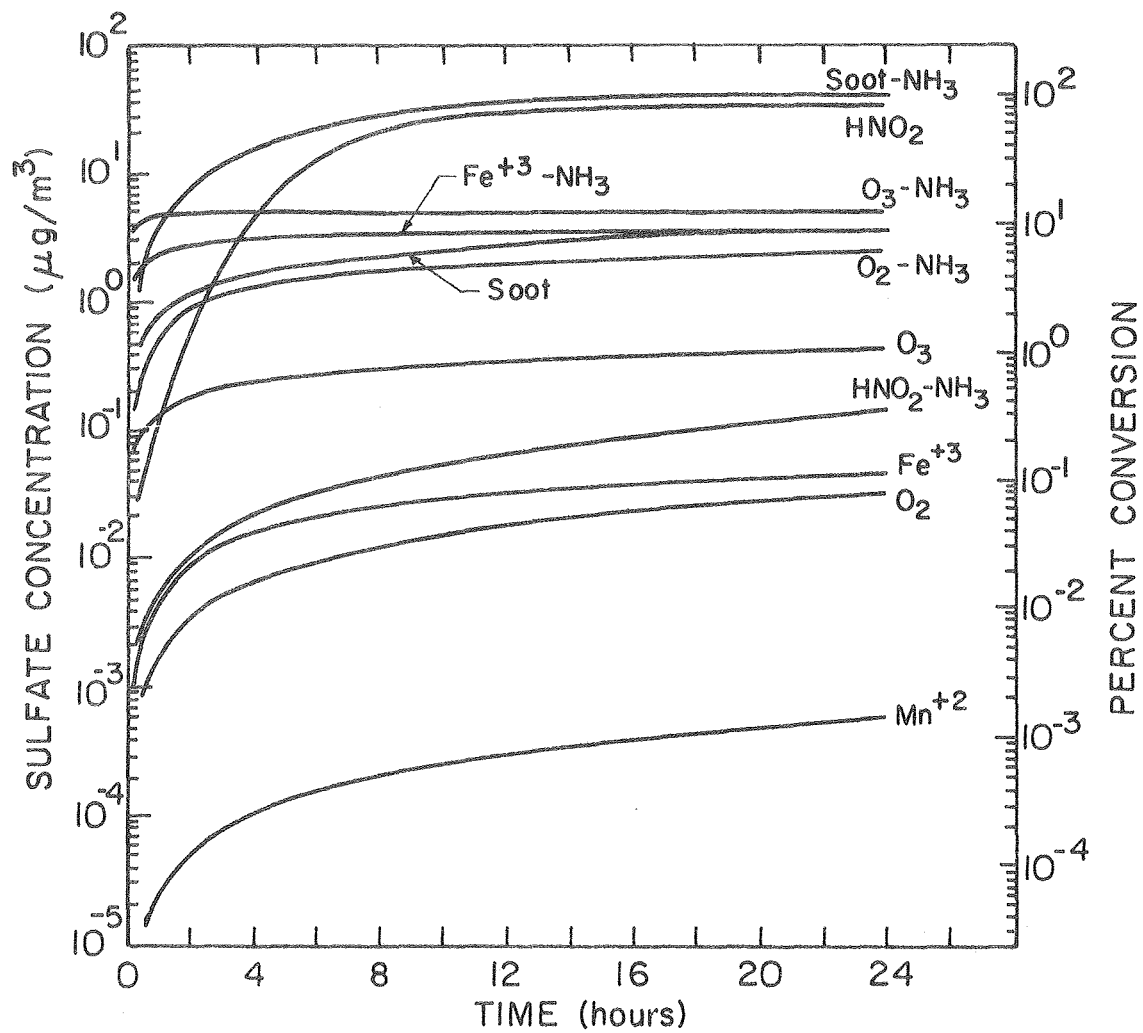
XBL808-5732

Figure 10



XBL 808-5733

Figure 11



XBL808-5735

Figure 12

